Continental Shelf Research 184 (2019) 21–29

Contents lists available at ScienceDirect

Continental Shelf Research

journal homepage: www.elsevier.com/locate/csr

Spatiotemporal variation in summer net community production in the Amundsen Sea Polynya: A self-organizing map analysis approach

Keyhong Park[a], Doshik Hahm[b,*], Jung Ok Choi[a], Suqing Xu[c], Hyun-Cheol Kim[d], SangHoon Lee[a]

[a] Division of Polar Ocean Sciences, Korea Polar Research Institute, Incheon, 21990, South Korea
[b] Department of Oceanography, Pusan National University, Busan, 46241, South Korea
[c] Key Laboratory of Global Change and Marine-Atmospheric Chemistry, Third Institute of Oceanography, Ministry of Natural Resources, Xiamen, 361005, PR China
[d] Unit of Arctic Sea-Ice Prediction, Korea Polar Research Institute, Incheon, 21990, South Korea

ARTICLE INFO

Keywords:
Amundsen sea polynya
Net community production
Self-organizing map
Southern ocean
Primary production
Biological pump

ABSTRACT

We estimated weekly summer net community production (NCP) in the Amundsen Sea Polynya for 2010–2011 and 2011–2012 using the self-organizing map analysis technique, which is a type of artificial neural network useful for discovering underlying structure in datasets. The net community production estimates derived with four variables (sea surface temperature, mixed layer depth, chlorophyll-*a*, and photosynthetically available radiation) robustly reproduced the observed net community production in the Amundsen Sea Polynya. The mean net community productions were estimated as 0.42 ± 0.09 and 0.39 ± 0.07 gC $m^{-2} d^{-1}$ in 2010–2011 and 2011–2012, respectively. The maximum weekly net community production of 1.29 gC $m^{-2} d^{-1}$ in 2011–2012 was greater than in 2010–2011 by 0.32 gC $m^{-2} d^{-1}$. The net community production in 2010–2011, derived using the self-organizing map, showed weekly variation similar to the trend of satellite-derived production of the *Eppley*-Vertically Generalized Production Model. However, in 2011–2012, it exhibited different temporal variation both in peak timing and in magnitude of the bloom. This implies the existence of complex processes not readily resolved by the four variables used in our self-organizing map analysis. Therefore, further observations during different blooming stages are required to improve self-organizing map-derived net community production estimates.

1. Introduction

In the Southern Ocean, primary production occurs predominantly in the continental shelf region, which is where phytoplankton blooms occur during austral summer when the sea ice melts and an ample amount of solar radiation is available at the sea surface. In particular, the Amundsen Sea Polynya (ASP) is the most productive polynya among the Antarctic coastal polynyas (Arrigo and van Dijken, 2003) because of relatively high light availability (Park et al., 2017) or enhanced iron supply (Thuróczy et al., 2012). In addition, the Amundsen Sea, embracing the ASP, is a region highly susceptible to the effects of current climate change, as evidenced by rapid glacial melting and sea surface temperature (SST) rise (Depoorter et al., 2013; Rignot et al., 2014; Stammerjohn et al., 2015).

Net community production (NCP) is the difference between net primary production (NPP) and heterotrophic respiration in the surface layer and it is considered a measure of the biological carbon pump (Alkire et al., 2012; Boss and Behrenfeld, 2010; Laws, 1991; Nicholson et al., 2012; Plant et al., 2016). Given the high primary production in coastal polynyas around Antarctica, which accounts for 65% of primary production on the continental shelves (Arrigo and van Dijken, 2003), the significance of polynyas as carbon sinks can be disproportionate. Thus, quantifying the magnitude of summer season NCP and its interannual variation in the Amundsen Sea is essential to understand the interplay between climate change and the biogeochemical carbon cycle in the Southern Ocean (Emerson, 2014; Eveleth et al., 2017; Nevison et al., 2012, 2018). For instance, NCP has been found correlated significantly with the Southern Annular Mode and El Niño-Southern Oscillation in the Western Antarctic Peninsula region (Li et al., 2016).

Self-organizing map (SOM) analysis is a type of artificial neural network that has been proven useful in extracting and classifying features in geoscience, e.g., the spatiotemporal patterns of wintertime surface temperature anomalies and climate extremes over Australia (Gibson et al., 2017; Huang et al., 2017). In oceanography, the SOM approach has been applied to analysis of various properties of seawater such as SST (Iskandar, 2010; Liu et al., 2006), chlorophyll

* Corresponding author.
E-mail address: hahm@pusan.ac.kr (D. Hahm).

https://doi.org/10.1016/j.csr.2019.07.001
Received 2 July 2018; Received in revised form 4 May 2019; Accepted 2 July 2019
Available online 06 July 2019
0278-4343/

concentration (Huang et al., 2017a; Silulwane et al., 2001), and pCO_2 (Landschützer et al., 2013; Laruelle et al., 2017; Xu et al., 2019), and so on. Because the SOM algorithm does not require *a priori* description of the relationship between input and output data, i.e., unsupervised learning, it enables us to estimate phenomena from parameters whose relationships are not described adequately by mathematical equations. Thus, it is particularly useful to expand on the spatiotemporal coverage of direct measurements or to estimate properties for which satellite observations are technically limited. Some previous studies have suggested that applying a region-specific algorithm, instead of a single global algorithm, better reflects the characteristics of the seas and produces estimates of NCP or pCO_2 that are more reliable (Hales et al., 2012; Li and Cassar, 2016).

Previously, several modeling studies have reported NCP estimates in the Southern Ocean using various techniques such as a carbon-based NPP model (Westberry et al., 2012), 3-D inverse model (Schlitzer, 2002), and vertically generalized production model (VGPM) NPP and export model (Nevison et al., 2012). Despite the importance of NCP to our understanding of the biogeochemical cycle of the ocean, its complex characteristics mean it is neither possible to observe NCP by satellite nor are there competent numerical models available to predict NCP reliably. Chang et al. (2014) were first to propose adopting SOM analysis for the estimation of NCP. They estimated the mean Southern Ocean NCP as 17.9 mmolC $m^{-2} d^{-1}$, with the range of the model-based estimates between 8.3 and 24 mmolC $m^{-2} d^{-1}$. Their estimation of NCP in the Southern Ocean using satellite- (chlorophyll-*a* (CHL) and photosynthetically available radiation (PAR)) and model-derived (mixed layer depth (MLD)) variables demonstrated that the SOM approach is feasible for overcoming the spatiotemporal limitations of *in situ* observations.

During austral summer in 2011 and 2012, we conducted underway observations of NCP of the Amundsen Sea (Hahm et al., 2014). Our investigations revealed large spatiotemporal variation of NCP in the ASP during the cruises; however, the duration of each study period was less than 2 weeks. Despite the importance of NCP for understanding the biological carbon cycle of the ocean, the spatiotemporal coverage of our observations was insufficient to capture and reveal the variation of NCP in the Amundsen Sea throughout the summer season when the polynya is open. Thus, we adopted SOM analysis to expand our observed datasets and to estimate weekly NCP maps during the summer season.

This study focused on presenting a robust method with which to estimate NCP in the ASP during summer. Therefore, not only do we suggest a variable set that optimally delineates the observed variation of NCP in the ASP, but we also estimate the temporal variation and spatial distribution of summer season NCP in the ASP.

2. Data and method

The tracks of *in situ* observations acquired during the cruises of the ice breaker R/V *Araon* (Hahm et al., 2014) and the prescribed ASP area (71°–75°S, 110°–120°W) for the NCP analyses are presented in Fig. 1. The NCP estimates from the SOM analysis were made for the two summer seasons: November 2010–March 2011 and November 2011–March 2012. In the SOM analysis, it was assumed that NCP had nonlinear relationships among the multiple estimators, e.g., such as photosynthetically available radiation (PAR), chlorophyll-a (CHL), sea surface temperature (SST), and mixed layer depth (MLD). These are some of the data available through satellite observations or model experiments, exploited for the prediction of NCP or pCO_2 values (Chang et al., 2014; Landschuster et al., 2014; Li and Cassar, 2016).

The SOM analysis used in this study was an adaptation of a previous approach established for estimates of NCP and pCO_2 (Chang et al., 2014; Telszewski et al., 2009; Xu et al., 2019). Briefly, our SOM analysis comprised three steps: training, labeling, and mapping (Fig. 2). Before running the SOM analysis, input variables to estimate NCP were prepared in vector form. During the training step, each neuron of the SOM

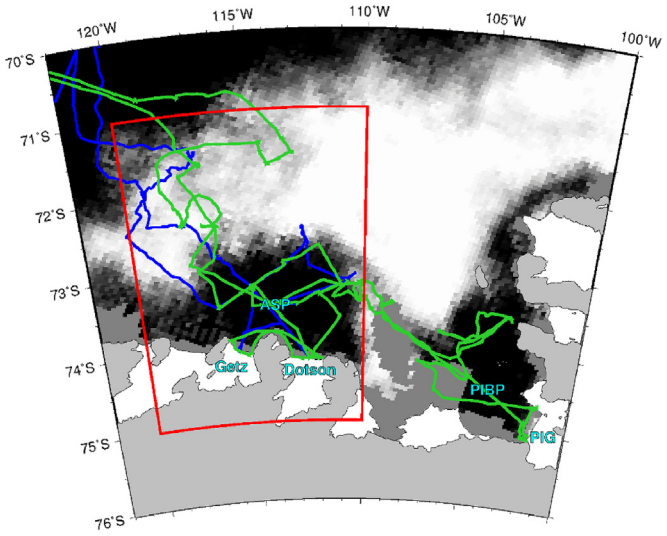

Fig. 1. Prescribed ASP area (red square) and cruise tracks of *in situ* measurements made during austral summer: blue and green lines represent 12/30/2010–1/8/2011 and 2/9/2012–3/6/2012, respectively. Sea ice concentration during 1/1/2011–1/8/2011 (week 5) is displayed over the map. (For interpretation of the references to color in this figure legend, the reader is referred to the Web version of this article.)

was tuned to represent a feature of the distribution of input vectors. The labeling step labeled NCP values to the neurons based on our *in situ* input variables and NCP values (labeling datasets). Finally, the neurons assigned their representative NCP values to the relevant input vectors, following which the estimated NCP values in the vectors were gridded into a map (mapping procedure). We used the MATLAB SOM Toolbox 2.0 (Vesanto, 2002) for the analysis, which has been developed by the Laboratory of Computer and Information Science at the Helsinki University of Technology (http://www.cis.hut.fi/projects/somtoolbox).

2.1. Training step datasets

The following datasets were used as input variables for the analysis: MODIS Level-3 satellite images of SST, CHL, and PAR and GLobal Ocean ReanalYses and Simulations (GLORYS) MLD (Ferry et al., 2010)). The horizontal resolution of the input variables was set to 0.1° × 0.1°, and the input variables including *in situ* observation of NCP were re-gridded to match this resolution. The temporal variation of NCP was estimated for 8-day intervals, matching the intervals of the 8-day composite satellite products (SST, PAR, and CHL). Here, for convenience, each 8-day interval is referred to as a 'week' and numbered consecutively from 1 to 26 for 2010–2011 (weeks 1–12) and 2011–2012 (weeks 13–26). Complete information regarding the week index is given in Table S1.

2.2. Labeling step datasets

We used *in situ* values of SST, CHL, and NCP (Hahm et al., 2014) and MODIS and GLORYS products for PAR and MLD information, respectively. The PAR and MLD information was interpolated temporally and the nearest grid value was selected based on the spatiotemporal information of the *in situ* variables. In the SOM analyses, input vectors with missing elements were excluded, and we took 10-min averages of the values for the labeling step to minimize possible fitting noise or outliers.

2.3. Data coverage analysis

The statistics and range of the values of each variable are presented

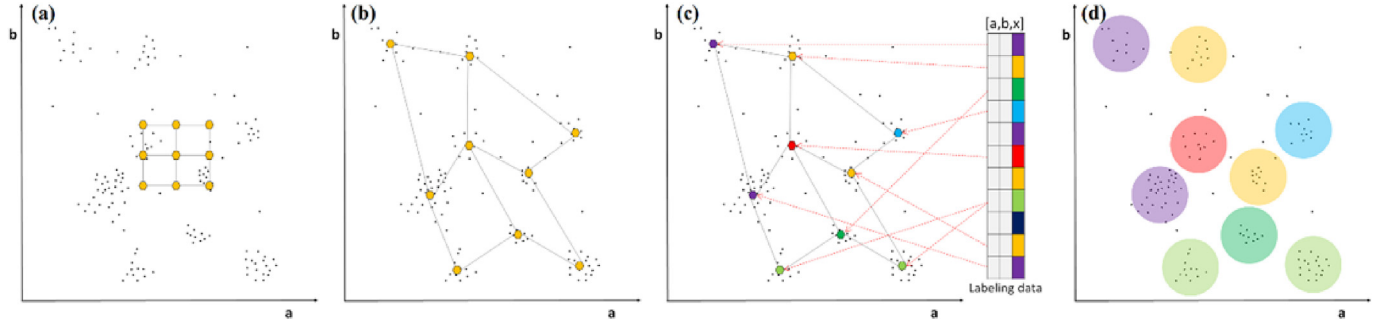

Fig. 2. Diagrams illustrating the SOM analysis procedure for a 2-D input vector case [a, b]: two input variables. Small dots are input vectors containing two elements (input variables) and the yellow dots are the SOM neurons (a). The training procedure extracts characteristics of the input variables and trains the neurons (b). During the labeling procedure, the property to be estimated (denoted as 'x') is labeled to the neurons from the labeling dataset (c). The mapping procedure assigns the labeled properties to the input vectors (d). (For interpretation of the references to color in this figure legend, the reader is referred to the Web version of this article.)

Table 1
Statistics of labeling and training datasets showing the distribution and coverage of each variable.

		SST	CHL	MLD	PAR
Labeling	*Max*	0.4	12.6	36.1	61.5
	min	−1.8	0.8	12.2	4.6
	mean	−1.1	4.9	20.3	28.0
	Skewness	0.7 (0.3)[a]	0.6 (−0.5)	0.3 (0.2)	0.0 (−1.1)
Training	*Max*	2.2	36.6	186.4	65.6
	Min	−1.9	0.1	9.4	1.6
	Mean	−0.6	2.4	23.8	36.9
	Skewness	0.7 (0.2)	3.3 (0.1)	3.3 (1.5)	0.1 (−0.9)
	N coverage[b] *(%)*	83.6 (98.1)[c]	63.1 (97.3)	69.3 (95.6)	97.3 (97.0)

The unit of each variable is °C (SST), mg m^{-3} (CHL), m (MLD), and Einstein $m^{-2} d^{-1}$ (PAR).

[a] The skewness of the common logarithm of each variable is shown in parentheses.

[b] ([number of training data within the labeling data range]/[total number of training data]) × 100.

[c] The percent labeling data coverage of normalized variables is shown in parentheses.

in Table 1. It is noted that our *in situ* datasets with NCP values for labeling do not cover the extremely high values of CHL and MLD used for training. This means NCP under extreme input variables might not be estimated optimally by the SOM analysis. NCP estimates that are more realistic could be expected from the SOM analysis when the distribution and variation range of the labeling variables reflect those of the training dataset more closely (Nakaoka et al., 2013). The CHL and MLD values displayed significant positive skewness. To make both the training and the labeling datasets close to a normal distribution, the common logarithm of the CHL and MLD values was used in the analyses. The data coverage of the training dataset of CHL and MLD by the labeling datasets was 63% and 69%, respectively, which might reflect insufficient spatiotemporal coverage and/or bias between the labeling and training datasets. Thus, this implies that the use of an adequate number of *in situ* observations in the SOM analysis would reproduce NCP estimates that are more realistic. However, before running the SOM analysis, we normalized the variables because this is a tenable method with which to resolve data coverage issues by significantly increasing the data coverage. Table 1 shows that the data coverage was evidently improved after normalization for all four variables. Also, another benefit of normalizing the input variables was that it enabled us to overcome the weighting issue. The weighting issue can produce biased SOM results because of the different magnitudes among the variables (Ultsch and Röske, 2002).

3. Optimization of input variable set

In order to estimate NCP in the ASP, we determined an optimum set of input variables through a bootstrapping analysis of different input variable sets. During this procedure (optimization), we tested the reproducibility of the SOM-derived NCP from the different sets of input variables, and we identified one set of input variables whose SOM-derived NCP was closest to the measured NCP. Four different sets of input variables were tested: SCP - [SST, CHL, PAR], CMP - [CHL, MLD, PAR], SCM - [SST, CHL, MLD], and SCMP - [SST, CHL, MLD, PAR]. SCP comprised the variables used to estimate primary production in the VGPM (Behrenfeld and Falkowski, 1997), and CMP comprised the variables suggested by Chang et al. (2014) to estimate NCP in the Southern Ocean. Additionally, as previous work has found that NCP has strong negative correlation with MLD (Csaar et al. (2011); Hahm et al., 2014), SCM and SCMP were also added to the test input variable sets.

The bootstrapping analysis was performed using NCP and input variables of the 2011 and 2012 observation periods. *In situ* measurements were used for NCP, SST, and CHL and MODIS satellite and GLORYS reanalysis results were applied for PAR and MLD, respectively. For each set of input variables, we selected at random 80% of the *in situ* measurements for training, and their corresponding observational NCP values were reserved to validate the SOM-derived NCP. The trained SOM was labeled using the measured NCP of the remaining 20% of *in situ* measurements. Then, the credibility of the SOM-derived NCP values was checked by comparison with the reserved NCP values. To determine the optimum input variable set, the bootstrapping analysis was iterated 30 times for each set. The outcome from the four sets of input variables is presented in Fig. 3.

The equality of *in situ* NCP (validation set) and SOM-derived NCP from the bootstrapping SOM runs was assessed by comparing the slopes and correlation coefficients between the two. While Chang et al. (2014) suggested that CMP is an optimum set of input variables with which to derive NCP in the Southern Ocean, we found that SCMP was the best estimator for the NCP values in the ASP. The slope and correlation coefficient between the SCMP-fed SOM-derived NCP values and those of the validation set was 0.86 ± 0.03 and 0.83 ± 0.02, respectively (Fig. S1). This implies that the best NCP estimates could be achieved when an input variable set is optimized for the physical and biogeochemical characteristics of the research area.

We also performed bootstrapping tests with different numbers of neurons (SOM size) to find the optimum number for the SOM analysis. The setup of the SOM analysis was the same as used for the input variable optimization but with the optimum set of input variables (SCMP). The four different numbers of neurons tested were 576 (determined using the heuristic formula, $SOM\ size = 5 \times [number\ of\ training\ data]^{1/2}$; Mari et al., 2010), 2048, 4096, and 8192. Excluding the 576 neuron case, which substantially underestimated (slope = 0.55) NCP during the bloom period (week index 5), the other

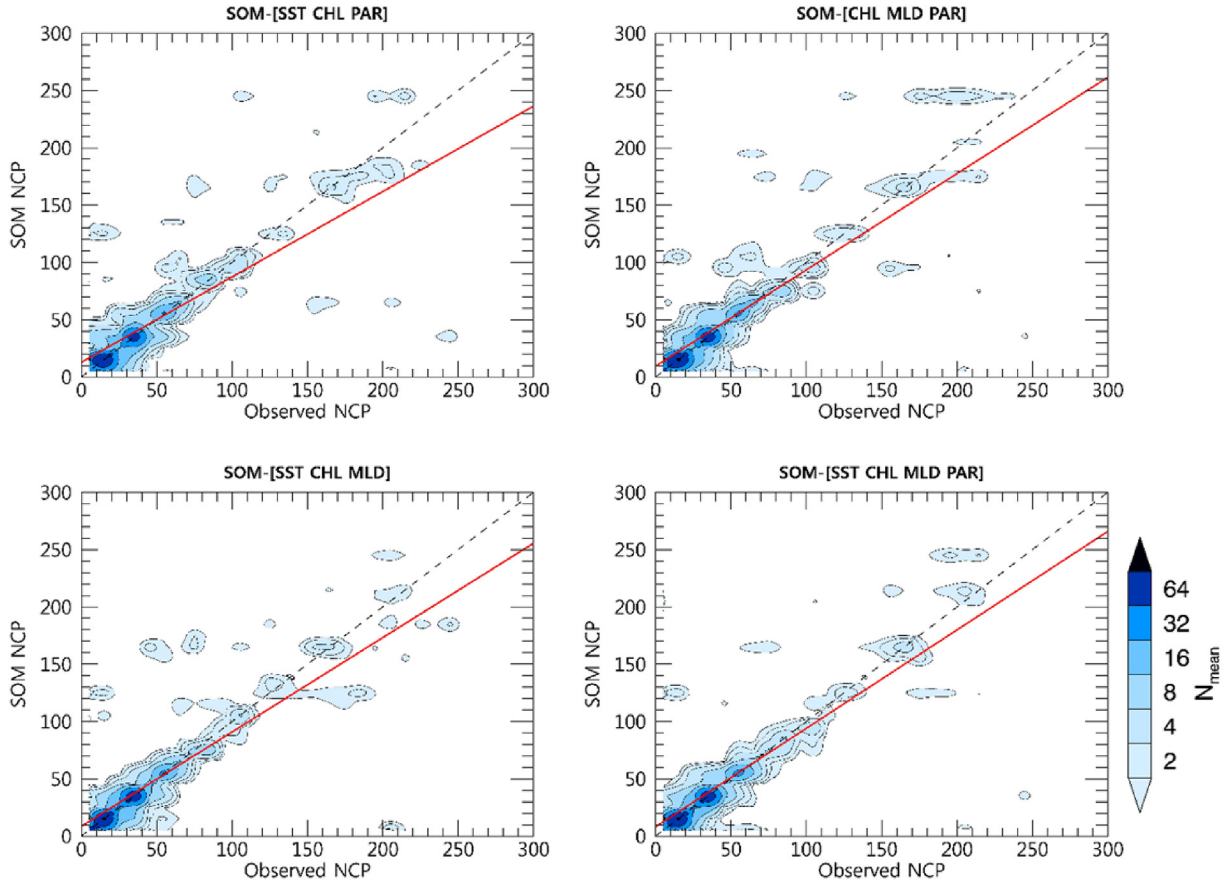

Fig. 3. Contoured 1-to-1 plots between observed and SOM-derived NCP from the four different variable sets. Each contoured plot is created using the mean appearance number of 30 bootstrapping analyses in bins of size 10 mmol O_2 m^{-2} day^{-1}. Gray dotted line is the 1-to-1 line and the red solid line is the regression line. (For interpretation of the references to color in this figure legend, the reader is referred to the Web version of this article.)

cases showed similar slope (≈1) and correlation (≈0.5) (Table S2). We selected the case of 4096 neurons for further analyses because it provided a reasonable balance between the validity of the prediction and the speed of the run.

4. Spatiotemporal variation of NCP in the Amundsen Sea Polynya

The SOM-derived NCP estimates are presented in Fig. 4 and Fig. S2. The SOM analysis utilized 8-day composite satellite and model input variables (Fig. 5 and Figs. S3–S6). In Fig. 4, the estimated NCP distribution in weeks 5 and 24 is compared with the observed NCP distribution. It is noted that there is a small temporal mismatch between the SOM-derived and the observed NCP. While the SOM-derived NCP values were calculated from the weekly composites of input variables, the *in situ* NCP was measured along the cruise track during the corresponding weeks. Despite this, the SOM-derived NCP estimates generally reproduce the *in situ* observations reasonably well. During week 5, NCP was enhanced in the western ASP and low NCP was found in the eastern ASP (Fig. 4(a) and (c)). In week 24, NCP was significantly lower than in week 5 throughout the polynya (Fig. 4(b) and (d)).

Assuming that the NCP/NPP ratio is ~0.5 (Hahm et al., 2014; Lee et al., 2012), the 'enhancement' of NCP is defined as NCP higher than 0.2 gC m^{-2} d^{-1} because Arrigo et al. (2012) defined the threshold of a bloom period as 0.4 gC m^{-2} d^{-1} of NPP. During austral summer in the ASP, the weekly estimated NCP distribution illustrated that NCP was enhanced with mean NCP greater than 25 mmol O_2 m^{-2} d^{-1} (~0.2 gC m^{-2} d^{-1}) during week 4–8 (December 19, 2010–February 1, 2011; 45 days) and week 16–22 (December 11, 2012–February 1, 2011; 53 days) (Fig. S2). During the two summer seasons, NCP enhancement occurred during the same period, i.e., week 3 (0.21 ± 0.01 gC m^{-2} d^{-1}) and week 16 (0.65 ± 0.07 gC m^{-2} d^{-1}) that correspond to December 11–18 of 2010 and 2011, respectively. This is comparable with Arrigo et al. (2012), who found uniform timing of the phytoplankton bloom in the ASP over a 13-year period. Additionally, once NCP enhancement began, it was found to appear promptly throughout the polynya, while subsidence tended to start from the margin.

The time series of weekly mean NCP estimates and SOM input variables in the ASP are presented in Fig. 6 and Table S3. The average NCP during the summer was 0.42 ± 0.09 gC m^{-2} d^{-1} in 2010–2011 (weeks 1–12) and 0.39 ± 0.07 gC m^{-2} d^{-1} in 2011–2012 (weeks 13–26). While the mean NCP values were similar, the NCP peak occurred 3 weeks earlier in 2011–2012 and its magnitude was 0.32 gC m^{-2} d^{-1} greater than in 2010–2011.

Overall, the time series of input variables also showed similar pattern and magnitude between the two years. In detail, the SST peak appeared approximately 2 weeks earlier in 2011–2012 than in 2010–2011. The CHL peak appeared approximately 1 week later in 2011–2012 than in 2010–2011, but the enhanced level of CHL was sustained longer, i.e., until mid-February. In both summers, the MLD shoaled rapidly during early December, which coincided with the beginning of the CHL bloom. The MLD remained shallow until the end of both summers. The temporal variation in PAR was similar in both years, although there were two dips in the 2011–2012 summer (i.e., weeks 17 and 19).

In the ASP, phytoplankton numbers start to increase as the extent of the sea ice rapidly decreases and the polynya begins to open in late November. Between early and mid-January, the bloom reaches its peak and then starts to subside because of nutrient limitation and

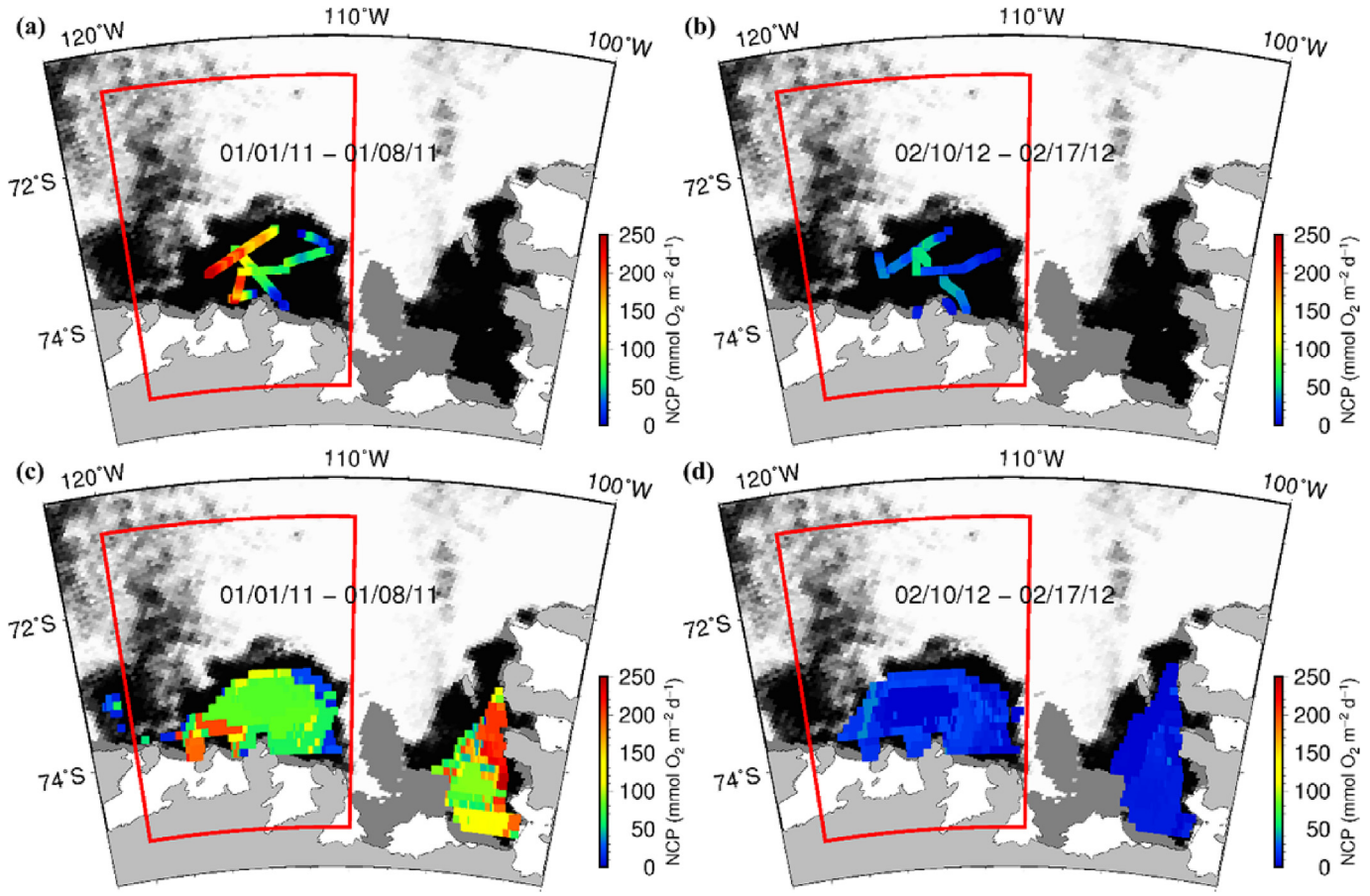

Fig. 4. (a) and (b) show the observed NCP in the Amundsen Sea Polynya and (c) and (d) show the SOM NCP estimates during the corresponding periods of weeks 5 and 24.

zooplankton grazing. At the end of February, the bloom ceases because of the reduction of solar radiation. In the ASP, this pattern of bloom have been taking place uniformly (Arrigo et al., 2012). As multiple environmental parameters control the phytoplankton bloom in the ASP, despite the similar blooming pattern of the two summers investigated in this study, interannual variation of the environmental parameters could have affected the difference in the timing of the peak between the two summers.

Robust correlation between MODIS SST and SOM-derived NCP was found throughout the summer in this study, consistent with previous *in situ* observations in the Pine Island Polynya (Tortell et al., 2012) and the ASP (Hahm et al., 2014). The variation of weekly mean NCP resembled that of SST, i.e., their peaks appeared 1–2 weeks earlier and they were higher in 2011–2012 in comparison with 2010–2011. The strong positive linear relationship ($r = 0.94$) found between weekly mean NCP and SST was more significant than that of the other input variables (Fig. S7). For instance, in the first week of January in both 2011 and 2012 (weeks 5 and 19), although the high NCP in week 19 was accompanied by high SST, the CHL, MLD, and PAR were similar or lower than in week 5. The correlation coefficients (r) between NCP and the other input variables were found moderate: 0.58, −0.69, and 0.56 for CHL, MLD, and PAR, respectively. Sometimes, it appeared input variables other than SST were more relevant to NCP variation, i.e., the NCP drop in week 17 was most likely affected by the sudden decrease in PAR.

The mean observed NCP in January 2011 was 1.02 ± 0.68 gC $m^{-2} d^{-1}$ (Hahm et al., 2014). The observation period was mostly covered by week 5. SOM-derived mean NCP in the week, 0.74 ± 0.14 gC m^{-2} d^{-1}, was approximately 30% lower than the observational mean value. However, considering the large spatial variation, as indicated by the standard deviation, the difference between the SOM-derived mean NCP and that of the *in situ* observations is marginal. The SOM-derived NCP was slightly less than observed in February 2012, i.e., the observed NCP was 0.20 ± 0.12 gC $m^{-2} d^{-1}$, while the mean SOM-derived NCP for the corresponding week (week 24) was 0.11 ± 0.01 gC $m^{-2} d^{-1}$. Thus, it also lay within the standard deviation of the observations. Furthermore, Lee et al. (2012) measured primary production in the ASP (2.2 ± 1.4 gC $m^{-2} d^{-1}$) during a period similar to week 5. Multiplied by *f-ratios* in the range 0.43–0.60 (Hahm et al., 2014), the primary production yielded NCP values in the range 0.95–1.32 gC $m^{-2} d^{-1}$. The SOM-derived NCP in week 5 (0.74 gC $m^{-2} d^{-1}$) is 22% below the lower limit of estimated NCP (0.95 gC $m^{-2} d^{-1}$) calculated from NPP of Lee et al. (2012).

Previous studies have suggested significant spatiotemporal variability in biological processes. For example, estimates of daily mean primary production in the ASP have shown significant subweekly-scale variation (Arrigo et al., 2012). The chlorophyll-*a* observations using autonomous underwater gliders have also revealed an evident heterogeneous spatial distribution in the ASP (Schofield et al., 2015). Furthermore, the supply of iron from melting sea ice and glacial meltwater can control phytoplankton blooms in Antarctic shelf waters (Gerringa et al., 2012; Sedwick and DiTullio, 1997) and thus influence the temporal variation of NCP (Hahm et al., 2014). Given the circumstances, it is likely that there is significant temporal variability in NCP.

The temporal variability of SOM-derived NCP was compared with NCP values deduced using the *Eppley*-VGPM (Behrenfeld and Falkowski, 1997; Carr et al., 2006) (Fig. 7 and Table S3). The basis of the *Eppley*-VGPM is the standard VGPM, which calculates primary production from SST, CHL, and PAR information. However, instead of using a polynomial description of optimal assimilation efficiency (P^B_{opt}), it uses the exponential relationship described by Morel (1991), which is based on

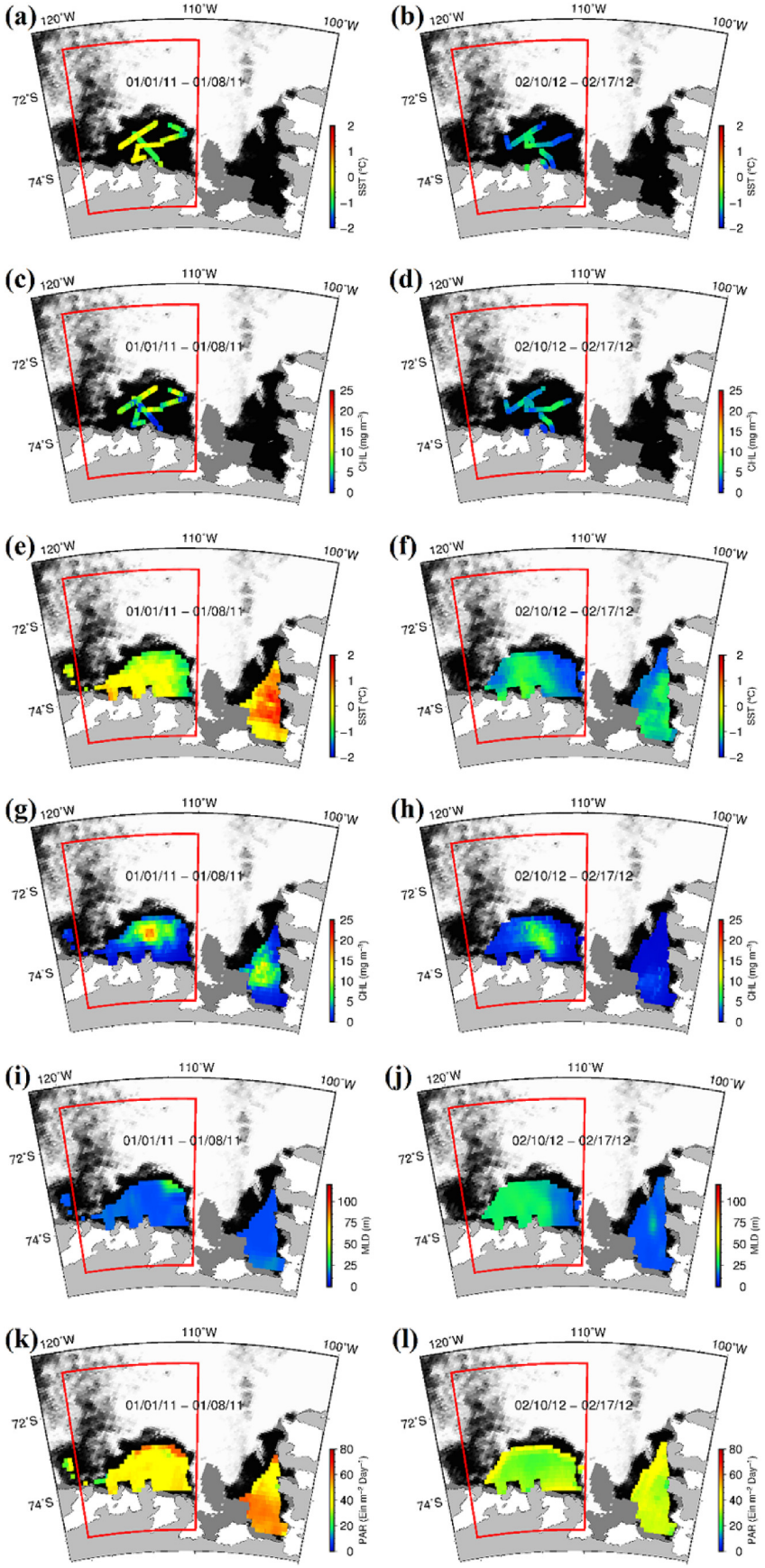

Fig. 5. Observed SST (a, b) and CHL (c, d) during weeks 5 and 24. Satellite or model input variables (SST, CHL, MLD, and PAR) for the SOM NCP estimation are presented in (e, g, i, and k) and (f, h, j, and l) for weeks 5 and 24, respectively.

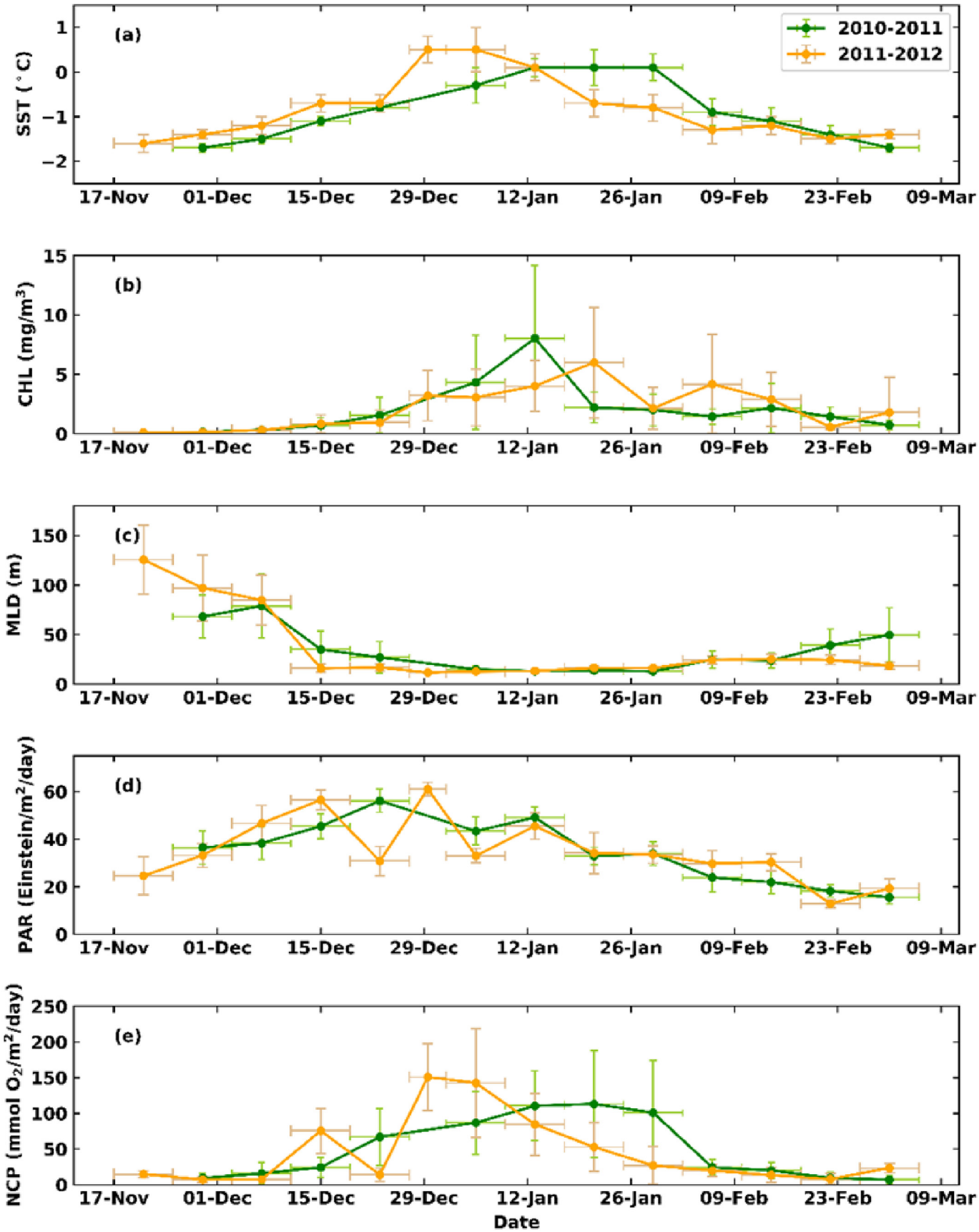

Fig. 6. Time series of weekly ASP mean SOM-derived NCP and input variables for SOM. Green lines represent summer 2010–2011 (weeks 1–12) and orange lines represent summer 2011–2012 (weeks 13–26). The x-axis error bars show the 8-day periods of each 'week,' but for week 18, it is just a 5-d period. The y-axis error bars represent 1-σ of each variable. (For interpretation of the references to color in this figure legend, the reader is referred to the Web version of this article.)

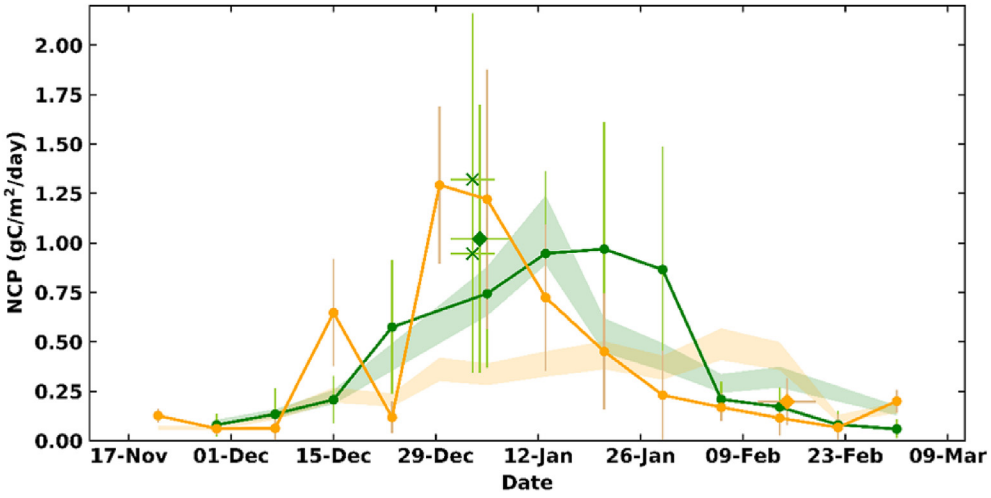

Fig. 7. Comparisons of ASP NCP values during summer 2010–2011 and 2011–2012. Green and orange colors represent the values in 2010–2011 and 2011–2012, respectively. Solid lines are SOM-derived NCP and shaded areas represent the *Eppley*-VGPM-derived NCP, which applied the same method as in (Hahm et al., 2014) [*NPP* × *f-ratio* (0.6 or 0.43)]. Green and orange diamonds are observed ASP NCP reported in (Hahm et al., 2014), and the two green crosses are NCP derived from NPP reported in (Lee et al., 2012), multiplied by a factor of 0.6 or 0.43 (*f-ratios*). All error bars are 1-σ of each dataset. (For interpretation of the references to color in this figure legend, the reader is referred to the Web version of this article.)

the curvature of the temperature-dependent growth function described by Eppley (1972). The *Eppley*-VGPM-derived NCP is calculated by multiplying primary production by constant *f-ratios* throughout the summer season. It should be noted that the validity of the *Eppley*-VGPM in the ASP or of the adoption of temporally invariant *f-ratios* is uncertain and it should be explored in future study.

The shaded areas in Fig. 7 indicate weekly ASP mean NCP estimates derived from the *Eppley*-VGPM for 2010–2011 and 2011–2012. The upper and lower boundary of each area is calculated by applying two fixed *f-ratios*: 0.43 and 0.6 (Hahm et al., 2014). Hahm et al. (2014) derived the lower and upper limits based on an empirical equation that predicts the *f-ratios* using SST and CHL as variables (Dunne et al., 2005) and *in situ* observations (Lee et al., 2012), respectively. During summer 2010–2011, the *Eppley*-VGPM-derived NCP and SOM-derived NCP were in accord until mid-January. However, the *Eppley*-VGPM-derived NCP dropped quickly after reaching a maximum at week 6, while the SOM-derived NCP remained high for a further 2 weeks before it subsided rapidly. In the following summer, the two estimates were too complex for reasonable comparison. The SOM-derived NCP showed a peak from late December to early January, whereas the *Eppley*-VGPM-derived NCP showed only a weak NCP peak in mid-February and attenuated NCP enhancement throughout the entire summer. Previous studies (Cassar et al., 2011; Hahm et al., 2014; Huang et al., 2012) and this study (Fig. S7) have found that MLD has a clear role in explaining NCP, i.e., a shallower MLD results in higher NCP. However, MLD information is not parameterized in the *Eppley*-VGPM, which implies that MLD played a more important role in calculating the NCP estimates in summer 2011–2012 than in 2010–2011.

5. Concluding remarks

The ASP is the most productive of the Antarctic coastal polynyas (Arrigo and van Dijken, 2003). However, there have been few investigations either of the underlying processes controlling phytoplankton blooms or of the efficiency of the biological pump in the ASP because of limited accessibility. To overcome the spatiotemporal limitation of *in situ* observations, we implemented SOM analysis, which is a type of artificial neural network method, using input variables acquired from satellite observations and modeling results.

Among the various input variables, the set of SST, CHL, MLD, and PAR was found to reproduce the observed ASP NCP appropriately in the SOM analysis. Based on our analysis, we presented, for the first time, the weekly spatiotemporal variation of NCP in the ASP during austral summer. The SOM-derived mean NCP was 0.42 ± 0.09 and 0.39 ± 0.07 gC m^{-2} d^{-1} for 2010–2011 and 2011–2012, respectively. In the ASP, SST showed a predominant role for controlling NCP (r = 0.94), and MLD showed the next strongest correlation with NCP (r = −0.69). Notwithstanding the large spatiotemporal variability of ASP NCP, comparisons between the SOM-derived NCP and the observational NCP showed at least approximately 20% underestimation of SOM-derived NCP. Hence, this implies a necessity of additional ASP NCP observation in a broader space and over longer time periods for a more reliable SOM based NCP estimate and its validation.

Comparison between the SOM-derived and *Eppley*-VGPM-derived NCP revealed a similar trend in 2010–2011 but significant discrepancy in 2011–2012. This elucidated the importance of MLD in understanding the biogeochemical cycle in polynyas (Arrigo et al., 2015), and implied the need for further effort to obtain a more realistic representation of modeled MLD. Additionally, Arrigo et al. (2015) suggested the basal melting rate of ice shelves cold be a key parameter in interpreting the high productivity of Antarctic coastal polynyas. Thus, incorporation of additional promising input variables in the current SOM method could improve the reproducibility of NCP estimates and enable us to understand the variation of polynya NCP more comprehensively.

Acknowledgements

This work was mainly supported by Korea Polar Research Institute grants (PE19060 and PE19120). Additionally, S. Xu was supported by the Scientific Research Foundation of Third Institute of Oceanography, MNR, No.2019008 S and the Qingdao National Laboratory for marine science and technology (No. QNLM2016ORP0109). All observational datasets and SOM modeling results are available upon request to the corresponding author (hahm@pusan.ac.kr).

Appendix A. Supplementary data

Supplementary data to this article can be found online at https://doi.org/10.1016/j.csr.2019.07.001.

References

Alkire, M.B., D'Asaro, E., Lee, C., Jane Perry, M., Gray, A., Cetinić, I., Briggs, N., Rehm, E., Kallin, E., Kaiser, J., González-Posada, A., 2012. Estimates of net community production and export using high-resolution, Lagrangian measurements of O2, NO3−, and POC through the evolution of a spring diatom bloom in the North Atlantic. Deep Sea Res. Oceanogr. Res. Pap. 64, 157–174.
Arrigo, K.R., Lowry, K.E., van Dijken, G.L., 2012. Annual changes in sea ice and phytoplankton in polynyas of the Amundsen Sea, Antarctica. Deep Sea Res. Part II Top. Stud. Oceanogr. 71, 5–15.
Arrigo, K.R., van Dijken, G.L., 2003. Phytoplankton dynamics within 37 Antarctic coastal polynya systems. J. Geophys. Res.: Oceans 108.
Arrigo, K.R., van Dijken, G.L., Strong, A.L., 2015. Environmental controls of marine productivity hot spots around Antarctica. J. Geophys. Res.: Oceans 120, 5545–5565.
Behrenfeld, M.J., Falkowski, P.G., 1997. Photosynthetic rates derived from satellite-based

chlorophyll concentration. Limnol. Oceanogr. 42, 1–20.
Boss, E., Behrenfeld, M., 2010. In situ evaluation of the initiation of the North Atlantic phytoplankton bloom. Geophys. Res. Lett. 37 n/a-n/a.
Carr, M.-E., Friedrichs, M.A.M., Schmeltz, M., Noguchi Aita, M., Antoine, D., Arrigo, K.R., Asanuma, I., Aumont, O., Barber, R., Behrenfeld, M., Bidigare, R., Buitenhuis, E.T., Campbell, J., Ciotti, A., Dierssen, H., Dowell, M., Dunne, J., Esaias, W., Gentili, B., Gregg, W., Groom, S., Hoepffner, N., Ishizaka, J., Kameda, T., Le Quéré, C., Lohrenz, S., Marra, J., Mélin, F., Moore, K., Morel, A., Reddy, T.E., Ryan, J., Scardi, M., Smyth, T., Turpie, K., Tilstone, G., Waters, K., Yamanaka, Y., 2006. A comparison of global estimates of marine primary production from ocean color. Deep Sea Res. Part II Top. Stud. Oceanogr. 53, 741–770.
Cassar, N., DiFiore, P.J., Barnett, B.A., Bender, M.L., Bowie, A.R., Tilbrook, B., Petrou, K., Westwood, K.J., Wright, S.W., Lefevre, D., 2011. The influence of iron and light on net community production in the Subantarctic and Polar Frontal Zones. Biogeosciences 8, 227–237.
Chang, C.H., Johnson, N.C., Cassar, N., 2014. Neural network-based estimates of Southern Ocean net community production from in situ O_2/Ar and satellite observation: a methodological study. Biogeosciences 11, 3279–3297.
Depoorter, M.A., Bamber, J.L., Griggs, J.A., Lenaerts, J.T.M., Ligtenberg, S.R.M., van den Broeke, M.R., Moholdt, G., 2013. Calving fluxes and basal melt rates of Antarctic ice shelves. Nature 502, 89–92.
Emerson, S., 2014. Annual net community production and the biological carbon flux in the ocean. Glob. Biogeochem. Cycles 28, 14–28.
Eveleth, R., Cassar, N., Sherrell, R.M., Ducklow, H., Meredith, M.P., Venables, H.J., Lin, Y., Li, Z., 2017. Ice melt influence on summertime net community production along the Western Antarctic Peninsula. Deep Sea Res. Part II Top. Stud. Oceanogr. 139, 89–102.
Ferry, N., Parent, L., Garric, G., Barnier, B., Jourdain, N.C., the Mercator Ocean team, 2010. Mercator global eddy permitting ocean reanalysis GLORYS1V1: description and results. Mercat. Q. Newsl. 36, 15–27.
Gerringa, L.J.A., Alderkamp, A.-C., Laan, P., Thuróczy, C.-E., De Baar, H.J.W., Mills, M.M., van Dijken, G.L., Haren, H.v., Arrigo, K.R., 2012. Iron from melting glaciers fuels the phytoplankton blooms in Amundsen Sea (Southern Ocean): iron biogeochemistry. Deep Sea Res. Part II Top. Stud. Oceanogr. 71–76, 16–31.
Gibson, P.B., Perkins-Kirkpatrick, S.E., Uotila, P., Pepler, A.S., Alexander, L.V., 2017. On the use of self-organizing maps for studying climate extremes. J. Geophys. Res.: Atmosphere 122, 3891–3903.
Hahm, D., Rhee, T.S., Kim, H.-C., Park, J., Kim, Y.-N., Shin, H.C., Lee, S., 2014. Spatial and temporal variation of net community production and its regulating factors in the Amundsen Sea, Antarctica. J. Geophys. Res.: Oceans 119, 2815–2826.
Hales, B., Strutton, P.G., Saraceno, M., Letelier, R., Takahashi, T., Feely, R., Sabine, C., Chavez, F., 2012. Satellite-based prediction of pCO_2 in coastal waters of the eastern North Pacific. Prog. Oceanogr. 103, 1–15.
Huang, J., Xu, F., Zhou, K., Xiu, P., Lin, Y., 2017a. Temporal evolution of near-surface chlorophyll over cyclonic eddy lifecycles in the southeastern Pacific. J. Geophys. Res.: Oceans 122, 6165–6179.
Huang, W., Chen, R., Yang, Z., Wang, B., Ma, W., 2017. Exploring the combined effects of the Arctic Oscillation and ENSO on the wintertime climate over East Asia using self-organizing maps. J. Geophys. Res.: Atmos. 122 (17), 9107–9129.
Huang, K., Ducklow, H., Vernet, M., Cassar, N., Bender, M.L., 2012. Export production and its regulating factors in the west Antarctica Peninsula region of the Southern Ocean. Glob. Biogeochem. Cycles 26.
Iskandar, I., 2010. Seasonal and interannual patterns of sea surface temperature in Banda Sea as revealed by self-organizing map. Cont. Shelf Res. 30, 1136–1148.
Landschützer, P., Gruber, N., Bakker, D.C.E., Schuster, U., Nakaoka, S., Payne, M.R., Sasse, T.P., Zeng, J., 2013. A neural network-based estimate of the seasonal to inter-annual variability of the Atlantic Ocean carbon sink. Biogeosciences 10, 7793–7815.
Laruelle, G.G., Landschützer, P., Gruber, N., Tison, J.L., Delille, B., Regnier, P., 2017. Global high resolution monthly pCO2 climatology for the coastal ocean derived from neural network interpolation. Biogeosci. Discuss.. 2017 1–40.
Laws, E.A., 1991. Photosynthetic quotients, new production and net community production in the open ocean. Deep Sea Research Part A. Deep-Sea Res. Part A Oceanogr. Res. Pap. 38, 143–167.
Lee, S.H., Kim, B.K., Yun, M.S., Joo, H., Yang, E.J., Kim, Y.N., Shin, H.C., Lee, S., 2012. Spatial distribution of phytoplankton productivity in the Amundsen Sea, Antarctica. Polar Biol. 35, 1721–1733.
Li, Z., Cassar, N., 2016. Satellite estimates of net community production based on O_2/Ar observations and comparison to other estimates. Glob. Biogeochem. Cycles 30, 735–752.
Li, Z., Cassar, N., Huang, K., Ducklow, H., Schofield, O., 2016. Interannual variability in net community production at the Western Antarctic Peninsula region (1997–2014). J. Geophys. Res.: Oceans 121, 4748–4762.
Liu, Y., Weisberg, R.H., He, R., 2006. Sea surface temperature patterns on the west Florida shelf using growing hierarchical self-organizing maps. J. Atmos. Ocean. Technol. 23, 325–338.
Nakaoka, S., Telszewski, M., Nojiri, Y., Yasunaka, S., Miyazaki, C., Mukai, H., Usui, N., 2013. Estimating temporal and spatial variation of ocean surface pCO_2 in the North Pacific using a self-organizing map neural network technique. Biogeosciences 10, 6093–6106.
Nevison, C., Munro, D., Lovenduski, N., Cassar, N., Keeling, R., Krummel, P., Tjiputra, J., 2018. Net community production in the Southern Ocean: insights from comparing atmospheric potential oxygen to satellite ocean color algorithms and ocean models. Geophys. Res. Lett. 45 (10), 510–549 559.
Nevison, C.D., Keeling, R.F., Kahru, M., Manizza, M., Mitchell, B.G., Cassar, N., 2012. Estimating net community production in the Southern Ocean based on atmospheric potential oxygen and satellite ocean color data. Glob. Biogeochem. Cycles 26 n/a-n/a.
Nicholson, D.P., Stanley, R.H.R., Barkan, E., Karl, D.M., Luz, B., Quay, P.D., Doney, S.C., 2012. Evaluating triple oxygen isotope estimates of gross primary production at the Hawaii Ocean Time-series and Bermuda Atlantic Time-series Study sites. J. Geophys. Res.: Oceans 117.
Park, J., Kuzminov, F.I., Bailleul, B., Yang, E.J., Lee, S., Falkowski, P.G., Gorbunov, M.Y., 2017. Light availability rather than Fe controls the magnitude of massive phytoplankton bloom in the Amundsen Sea polynyas, Antarctica. Limnol. Oceanogr. 62, 2260–2276.
Plant, J.N., Johnson, K.S., Sakamoto, C.M., Jannasch, H.W., Coletti, L.J., Riser, S.C., Swift, D.D., 2016. Net community production at Ocean Station Papa observed with nitrate and oxygen sensors on profiling floats. Glob. Biogeochem. Cycles 30, 859–879.
Rignot, E., Mouginot, J., Morlighem, M., Seroussi, H., Scheuchl, B., 2014. Widespread, rapid grounding line retreat of pine Island, thwaites, smith, and kohler glaciers, west Antarctica, from 1992 to 2011. Geophys. Res. Lett. 41, 3502–3509.
Schlitzer, R., 2002. Carbon export fluxes in the Southern Ocean: results from inverse modeling and comparison with satellite-based estimates. Deep Sea Res. Part II Top. Stud. Oceanogr. 49, 1623–1644.
Schofield, O., Miles, T., Alderkamp, A.-C., Lee, S., Haskins, C., Rogalsky, E., Sipler, R., Sherrell, R.M., Yager, P.L., 2015. *In situ* phytoplankton distributions in the Amundsen Sea Polynya measured by autonomous gliders. Elementa: Elementa: Sci.Anthropocene 3.
Sedwick, P.N., DiTullio, G.R., 1997. Regulation of algal blooms in Antarctic Shelf Waters by the release of iron from melting sea ice. Geophys. Res. Lett. 24, 2515–2518.
Silulwane, N.F., Richardson, A.J., Shillington, F.A., Mitchell-Innes, B.A., 2001. Identification and classification of vertical chlorophyll patterns in the Benguela upwelling system and Angola-Benguela front using an artificial neural network. S. Afr. J. Mar. Sci. 23, 37–51.
Stammerjohn, S.E., Maksym, T., Massom, R.A., Lowry, K.E., Arrigo, K.R., Yuan, X., Raphael, M., Randall-Goodwin, E., Sherrell, R.M., Yager, P.L., 2015. Seasonal sea ice changes in the Amundsen Sea, Antarctica, over the period of 1979–2014. Elementa: Elementa: Sci.Anthropocene 3.
Telszewski, M., Chazottes, A., Schuster, U., Watson, A.J., Moulin, C., Bakker, D.C.E., González-Dávila, M., Johannessen, T., Körtzinger, A., Lüger, H., Olsen, A., Omar, A., Padin, X.A., Ríos, A.F., Steinhoff, T., Santana-Casiano, M., Wallace, D.W.R., Wanninkhof, R., 2009. Estimating the monthly pCO_2 distribution in the North Atlantic using a self-organizing neural network. Biogeosciences 6, 1405–1421.
Thuróczy, C.-E., Alderkamp, A.-C., Laan, P., Gerringa, L.J.A., Mills, M.M., Van Dijken, G.L., De Baar, H.J.W., Arrigo, K.R., 2012. Key role of organic complexation of iron in sustaining phytoplankton blooms in the Pine Island and Amundsen Polynyas (Southern Ocean). Deep Sea Res. Part II Top. Stud. Oceanogr. 71–76, 49–60.
Ultsch, A., Röske, F., 2002. Self-organizing feature maps predicting sea levels. Inf. Sci. 144, 91–125.
Vesanto, J., 2002. Data Exploration Process Based on the Self − Organizing Map. the Finnish Academies of Technology.
Westberry, T.K., Williams, P.J.l.B., Behrenfeld, M.J., 2012. Global net community production and the putative net heterotrophy of the oligotrophic oceans. Glob. Biogeochem. Cycles 26.
Xu, S., Park, K., Wang, Y., Chen, L., Qi, D., Li, B., 2019. Variations in the summer oceanic pCO_2 and carbon sink in Prydz Bay using the self-organizing map analysis approach. Biogeosciences 16, 797–810.